Electromagnetic inductance tomography (EMT): sensor, electronics and image reconstruction algorithm for a system with a rotatable parallel excitation field

Z.Z.Yu
A.J.Peyton
L.A.Xu
M.S.Beck

Abstract: The main features and principle of operation of an electromagnetic inductance tomography system are described. The system can image the distribution of electrically conducting and/or magnetically permeable materials and is analogous to the other electrical tomography systems which measure capacitance or resistance. The paper presents a nonintrusive system with a rotatable parallel uniform excitation magnetic field which improves the detectability at the centre of the object space with respect to that near the periphery. The sensor construction, electronics design and image reconstruction are described. A novel electronic compensation scheme is used to condition the output signals from the sensor. This scheme subtracts the empty space background field measurements and consequently increases the overall dynamic range of the data acquisition system. An image reconstruction technique based on a correlation method is described and some images are presented.

1 Introduction

Electrical tomographic techniques, including electrical capacitance tomography (ECT), electrical resistance tomography (ERT) and electromagnetic inductance tomography (EMT), have been applied to a wide variety of diverse applications such as geological surveying,

functional imaging in medicine and industrial/process monitoring by using ERT. In the process field, electrical tomography has been used to monitor the distribution of the material in a range of equipment, for example, multiphase flows in pipelines, hydrocyclones and fluidised beds by using ECT and ERT. Despite their relatively modest image resolution, electrical methods have proved to be very useful because of their high imaging speeds, low cost, nonintrusive and non-hazardous attributes [1, 2]. The instruments used have taken measurements of either capacitance or resistance.

This paper describes EMT, an electrical tomography instrument which is based on the measurement of inductance. The instrument provides images based on the distribution of electrically conductive and magnetically permeable material within the object space. The development of EMT together with ECT and ERT provide three fundamental electrical tomography techniques based on the measurement of resistance, capacitance and now inductance; collectively, these are able to image the three passive electromagnetic properties of materials: electrical conductivity (σ) [3–5], electrical permittivity (ε) [6, 7] and now magnetic permeability (μ) [8, 9]. A brief summary of these techniques of ECT, ERT and EMT is shown in Fig. 1.
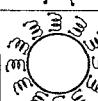
Tomographic Technique	Sensor type	Sensor arrangement	Measure Values	Range of property imaged	Typical material
Capacitance	Capacitive plates		Capacitance	Relative permittivity ε_r 10^0 to 10^2 Conductivity Low σ 10^{-1} S/m	Oil and water
Resistance	Electrodes		Resistance (Impedance)	Conductivity wide σ 10^{-1} to 10^7 S/m, Relative permittivity ε_r 10^0 to 10^2	Water/ saline
Electro-magnetic	Coils		Self/ Mutual Inductance	Conductivity High σ 10^2 to 10^7 S/m, Relative permeability μ_r 10^0 to 10^4	Metal/ minerals and water

Fig. 1 *Comparison of electrical tomography techniques*

In addition to the process visualisation applications mentioned above, there is a potential for the use of EMT where the material distribution can be characterised by its electrical conductivity or magnetic permea-

bility. Examples may include the tracking of ferrite labelled particles in transport and separation processes, foreign body detection and location, food inspection and validation of small metal components for defects. With modification it can be useful for imaging steel reinforcing bars inside concrete wall. The encouraging results [4] also suggest the possibility of imaging ionised water distributions within equipment and pipelines.

In common with the more established electrical tomography techniques, such as ECT [7] and ERT [10, 11], the EMT sensor also has poor relative detectability in the centre of the object space. This is true in general for all noninvasive electrical tomography sensors where the sensor elements are mounted on the boundary of the object space. For this reason, a parallel uniform excitation field is employed by the EMT system, which provides the strongest relative field in the centre of an electrical tomography system [13].

This paper presents an overview of the rotatable parallel uniform excitation field EMT system. The construction of the sensor and associated electronics are discussed, followed by a description of an image reconstruction algorithm which is based on a correlation method. Example images from the system are also presented.

2 System description

The EMT system consists of three main sub-systems shown in Fig. 2; the primary sensor, sensor electronics and image reconstruction computer. The primary sensor is built around a flanged section of plastic pipe, with an internal diameter of 150mm and length 500mm. The function of the sensor electronics is to control the sensor array, de dulate and condition the sensor output signals and interface the measured signals to the data conversion circuitry which is housed in the image reconstruction computer. This computer controls the measurement process and generates the images.
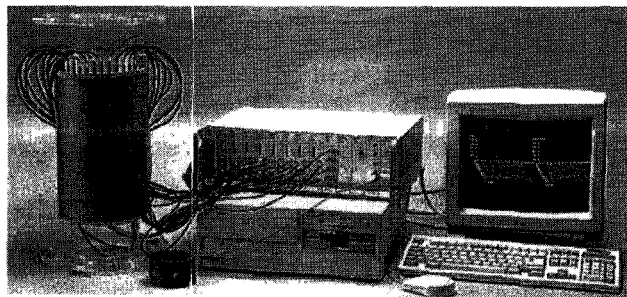
Fig. 2 *Photograph of the EMT system*
Left to right: sensor, electronics and image reconstruction computer

2.1 Sensor

One sensor requirement is to accurately detect the object field. This field is representative of variations to the homogeneity of the object space and hence the presence of conductive and/or ferrous/ferrite objects. A major consideration in the design of the sensor is to maximise the detectability. For an EMT sensor, detectability may be defined as the change in the output from a sensor coil with respect to a small perturbation in either permeability or conductivity in the object space. For material whose electromagnetic properties are linear, detectability is directly proportional to the magnitude of the object field which, in turn, is proportional to the magnitude of the excitation field. The

detectability in the central part of the object space can be improved with respect to the detectability at the periphery by increasing the relative field strength at the centre. Unfortunately, for the quasistatic conditions here, the magnetic field cannot be made greater in the centre than at the edge by using external excitation [12]. The uniform parallel situation is the optimum case in this respect.

For a circular object space, a parallel uniform magnetic field is generated by a sinusoidal distribution of current-turns around the boundary. Two sets of excitation coils, one of them shown in Fig. 3, were used, to generate uniform parallel magnetic fields in X and Y directions within the midsection of the (empty) object space. Each coil is driven by an independent voltage controlled current source. Computer control of the amplitude and phase (0° or 180°) of the currents in both coils allows the generation of a parallel field at any desired angle.
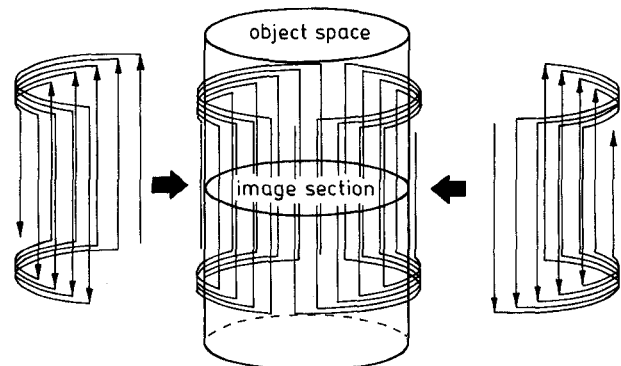
Fig. 3 *Excitation coil structure for generating a field in the x-direction*
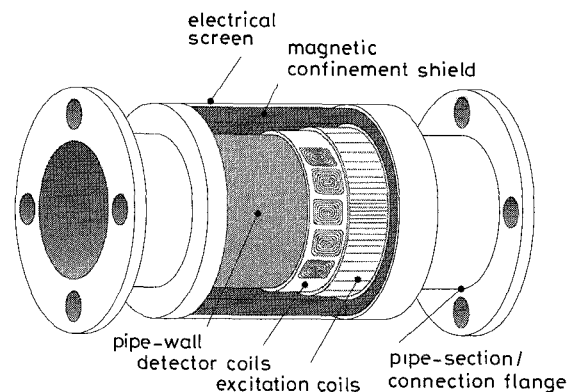
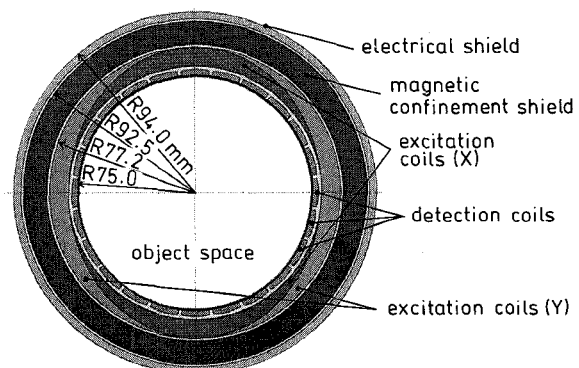**Fig. 4** *Structure of the primary sensor: cut-off view*

Fig. 5 *Structure of the primary sensor: cross-sectional structure*

The structure of the primary sensor is shown in Fig. 4. The cross-sectional structure of the sensor is shown in Fig. 5. The sensor itself has four subassem-

blies: the excitation coils, the detection coils, a magnetic confinement shield and an outer electrical screen.

There are 24 individual detection coils, equispaced around the circumference, to measure the peripheral flux density for each particular excitation field projection. Phase sensitive detection (PSD) is used, thus two signals (in-phase and quadrature) are obtained from each detection coil. Consequently, a combination of projections in the X and Y directions will give 48 independent in-phase measurements, and 48 independent quadrature measurements.

The magnetic confinement shield concentrates the field inside the image space and prevents interference from external sources. The shield is constructed from a ferrite powder/polypropylene composite material. The electrical screen further confines the flux and improves electromagnetic compatibility.

The sensor has two major features:

(i) A uniform parallel field provides the maximum relative field in the centre of the object space with respect to the peripheral field strength. With other excitation field patterns, the field strength is always larger close to the energising coil(s). As the detectability is proportional to the strength of the excitation field, a parallel field will therefore increase the detectability and SNR in the central region when compared to other excitation patterns.

(ii) Potential for fast data collection rates. A separate set of excitation coils are employed to generate the parallel field, thus the coils do not require a switching function between sensing and excitation modes as with many electrical tomography systems. All the sensing coils work concurrently while the excitation coils set the field projections. This enables simultaneous excitation and sensing, allowing parallel measurement of the detection signals. Using a fully parallel demodulation and digitisation scheme, the capture rate may be increased to 240 frame/sec.
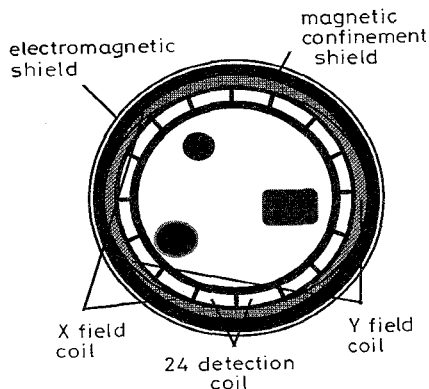

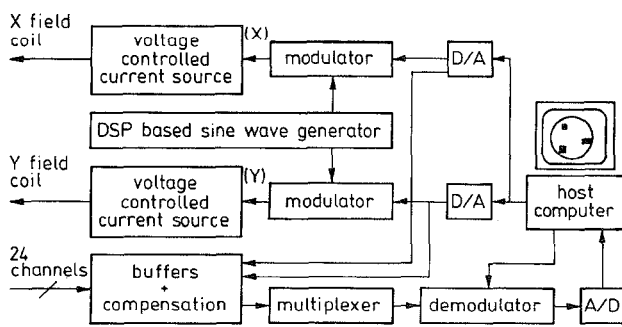
Fig. 6 *Electromagnetic tomography sensor*

Fig. 7 *Block diagram of electromagnetic tomography system*

2.2 Conditioning electronics

The sensor electronics is shown in block diagram form in Fig. 7. It has two main functions: (i) to control the excitation coils and (ii) to condition the outputs from the detection coils. The excitation circuitry contains a 156 kHz sine wave generator based on a digital signal processor, two modulators and two 12-bit digital-to-analogue converters (DACs). The 156 kHz sine wave is modulated by the outputs of two DACs which control the field strength and direction via two pairs of voltage-to-current converters which connect to the X and Y field coils shown in Fig. 7. The currents flowing in the excitation coils are:

$$I_x = I \sin \omega t \cos \vartheta \qquad (1)$$

$$I_y = I \sin \omega t \sin \vartheta \qquad (2)$$

where I is the current amplitude, ω is the angular frequency of the excitation field and ϑ is the angle of the projection.

The detection circuitry has 24 channels, each of which contains an input buffer and compensation circuitry. The channels are multiplexed to a PSD and subsequently digitised using a 12-bit analogue-to-digital converter (ADC). For each channel both the real and imaginary components are digitised.
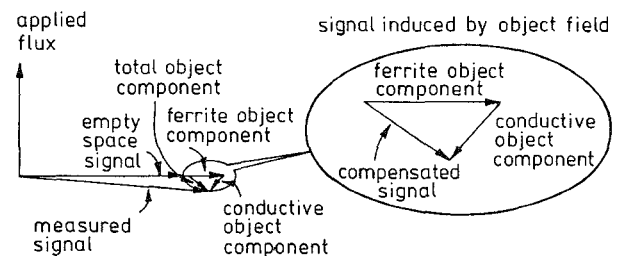

Fig. 8 *Phasor diagram of measured signal components*

When the object space is empty, the detector channels output relatively large empty space values which form a background measurement set. The output variations, caused by conductive or ferromagnetic objects, are relatively small compared to the background set; typically less than 25% when the object's size is less than 10% of the object space area. The large background signals reduce the effective range of the ADC (Fig. 7), and hence reduce the overall dynamic range of the data acquisition system. Fig. 8 shows a phasor diagram of the related signal components from the detection coil at 0° with 0° projection. The empty space signal (voltage) is lagging the excitation field, the applied flux, by 90°. The signal produced with material having a high permeability and low conductivity, such as ferrite, is in phase with the empty space signal. The signals produced from a conductive nonmagnetic object are lagging by an angle between 90° to 180°. The total component is a vector sum of the two which varies with the object distribution. It is important to measure both the phase and amplitude accurately, because small variations result from a large change to the object distribution. The compensation circuit subtracts the empty space signal from the measured signal, producing a compensated signal which represents a direct measurement of the object field. This enables the measurement of real and imaginary components of the object field.

A synthesised background signal for each channel can be obtained from the excitation signals shown in

22

IEE Proc.-Sci. Meas. Technol., Vol. 145, No. 1, January 1998

eqns. 1 and 2, and used to provide compensation. The block diagram of this compensation scheme for one channel at angle α is shown in Fig. 9.
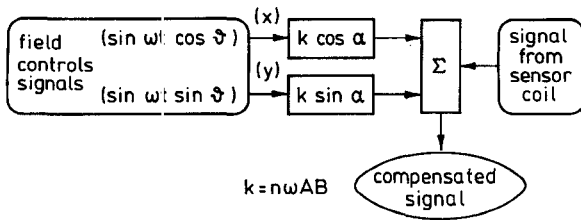

Fig.9 *Block diagram of the AC compensation scheme*

Each channel has its own compensation circuit which provides the following features:

(i) It can be tuned to compensate to within 1% of the empty space value for a chosen field projection angle and to within 5% for all other projections. The residual is then compensated in software.

(ii) The compensation signals tracks thermal variations in the system, as the source of the compensation signals are the excitation field control signals themselves.

(iii) Any sensing coil in the image plane can be compensated as long as the location of the coil is unaltered.

(iv) The compensation is performed simultaneously for all the channels, thus the sensor is capable of providing data in parallel, enabling high speed data collection.

(v) Both the real (in phase) and imaginary (quadrature) components of the object field signal can be obtained from the compensated signals.

(vi) The dynamic range of the sensor is improved by a factor of 20 when compared to operation without the compensation circuitry.

In other electrical tomography systems, hardware compensation of the background values has been reported. For example an ECT system [6] employs a multi-DAC system under computer control to subtract the appropriate base value from each rectified signal; this can be considered as a DC compensation scheme where the phase information is ignored. The EMT system here uses a phase sensitive scheme because this reflects electrical and magnetic properties of the object (see Fig. 8). The compensation scheme effectively subtracts the empty space sensor values, and leaves a residual which is only dependent upon the object. The system can readily detect a steel rod of 6 mm diameter (4% of object space diameter) in the centre of object space, where the SNR of the signal is about 4:1, the worst possible case.

3 Image reconstruction

A number of different reconstruction algorithms [2] have been used in electrical tomography including qualitative algorithms such as weighted back projection to more computationally intensive quantitative algorithms based on the solution of the forward problem. Similarly, for EMT, several different reconstruction algorithms have been considered including, simple heuristic methods, weighted back-projection and arithmetic reconstruction techniques (ART). The relative performance merits of the different algorithms in terms of spatial and contrast resolution and their computational requirements is still subject to on-going research. The algorithm used by this system has been selected as an

example to illustrate the operation of the system as a whole.

The image area was divided into 217 pixels as shown in Fig. 10. Each of the pixels is individually numbered. This kind of pixel layout has been chosen to increase the efficiency of image processing and storage.
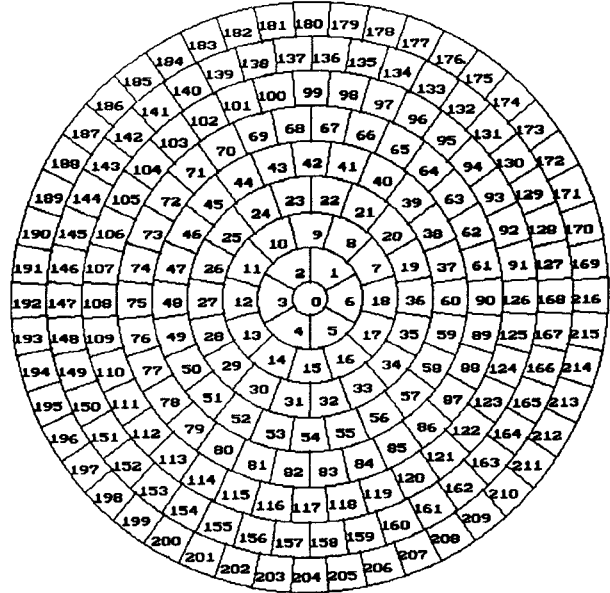

Fig.10 *Image pixels of the EMT system*

Image reconstruction was performed in two parts. First, collecting sensitivity data $y(p, c, n)$; the value measured by detection coil c in projection p, with the nth pixel occupied by a sample bar. This presampled data describes the response of the system to each individual pixel. Second, image reconstruction using a correlation technique, where the pre-sampled data $y(p, c, n)$ is correlated with the measured data $x(p, c)$. The reconstructed image $I(n)$ from P projections, is represented by pixel gray levels obtained by using the following expression, which gives the correlation.

$$I(n) =$$

$$\frac{\sum\limits_{i=1}^{24 \times P} x(p,c)y(p,c,n) - \frac{1}{24 \times P}\sum\limits_{i=1}^{24 \times P} x(p,c) \sum\limits_{i=1}^{24 \times P} y(p,c,n)}{\sqrt{\left[\sum\limits_{i=1}^{24 \times P} x(p,c)^2 - \frac{1}{24 \times P}\left(\sum\limits_{i=1}^{24 \times P} x(p,c)\right)^2\right] \times \left[\sum\limits_{i=1}^{24 \times P} y(p,c,n)^2 - \frac{1}{24 \times P}\left(\sum\limits_{i=1}^{24 \times P} y(p,c,n)\right)^2\right]}}$$

$$(3)$$

For six projections each frame of image takes 110ms on an IBM-compatible PC, with a 90MHz Pentium processor.

Fig. 11 (images 1 to 9) shows the reconstructed images when the bar is placed at various positions on the radius. To show the direct result of the correlation reconstruction method, no threshold was applied to artificially improve the appearance of the image. The grey levels from white to black represent correlation coefficients from 0 to 1. The image is well defined when the bar is near the edge (image 1), and sharpness drops as the bar moves towards the centre (image 9), the worst case. The reasons for the blurring effect are: (i) the correlation coefficient curve is not very sharp [14],
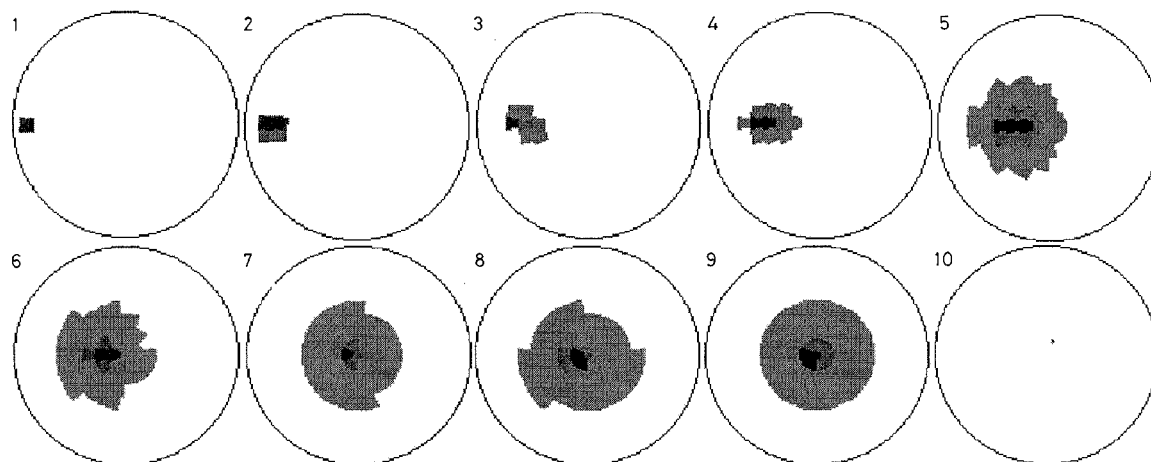
Fig. 11 *Reconstructed images of the sample bar in different positions by correlation algorithm*

and (ii) the sensitivity in the centre is lower than that near the edge. Despite these effects, the image contrast shows the correct object position by the darkest pixel. The appearance of an image can be further improved by applying a threshold filter to eliminate blurring around the object(s).

Image 10 is blank when a ferrite bar is in the object space as the image values are negative. If the map obtained using a conductive bar is used for image reconstruction, it will generate a negative image when measuring ferrite material in the object space. The converse is also valid when attempting to image conductive objects with a reference map using a ferrite object.

The correlation algorithm could be extended to image multiple objects, where additional signal patterns of multiobject distributions would be stored as a data map for correlation with the measured data. However, this would need considerably more computation and memory. Also, signal patterns tend to become less distinct when more objects are sampled which further limits the method. Despite this, the reconstruction method may be of use in applications where the object distribution is limited to specific patterns. For example, the detection of deviations from a normal standard product and for foreign body detection. In addition the method shows an ability for object identification. Therefore it is useful in identifying and locating a known object, conductive or ferrous.

4 Conclusions

This paper has presented one example of an EMT system with the largest relative excitation field strength in the centre of object space. The system has been developed in order to demonstrate the feasibility of using inductance for tomographic imaging and the method of generating rotatable parallel uniform excitation field. It also highlights the similarities between EMT and the other forms of electrical tomography such as ERT and ECT.

The system maximises the relative detectability and SNR in the centre of the object space. There is some evidence to suggest that for other electrical tomography techniques, a parallel uniform field may also be effective for object distinguishability [16]. However, the detectability in the centre is still lower than near the edge, as the object field drops with increasing distance. This is an inherent problem for nonintrusive electrical tomography systems.

The sensor has the potential to provide very fast frame data rates due to the smooth and rapid rotation of the excitation field. The separation of the excitation and detection sub-assemblies and parallel data collection are key design features required by a high speed tomography system. This can also be used in other types of electrical tomography systems. The empty space compensation scheme and phase sensitive detection of the object field are both important features of such a system.

A correlation image reconstruction algorithm has been developed. The signal patterns of one conductive bar at various positions were obtained by an experimental method, images have been shown by correlating 6 projections. It may be useful for the detection of known object(s). Therefore it can be used for tracking particular types of objects. Further development of a nonlinear complex reconstruction algorithm based on EM theory is expected in order to generate better images based on conductivity and ferromagnetic object content.

5 Acknowledgment

6 References

1 BECK, M.S., HOYLE, B.S., MORRIS, M.A., WATERFALL, R.C., and WILLIAMS, R.A.: 'Process tomography1995: Implementation for industrial processes'. 4th workshop on European concerted action on *Process tomography*, Bergen, Norway, March 1995

2 XIE, C.G.: 'Review of process tomography image reconstruction methods' in GRATTAN, K.T.V., and AUGOUSTI, A.T. (Eds.): 'Sensors VI: Technology, systems and applications' (IOP publishing, 1993), pp.341–346

3 DICKIN, F.J., HOYLE, B.S., HUNT, A., HUANG, S.M., ILYAS, O., LENN, C., WATERFALL, R.C., WILLIAMS, R.A., XIE, C.G., and BECK, M.S.: 'Tomographic imaging of industrial process equipment, techniques and applications', *IEE Proc. G*, Feb. 1992, **139**, (1), pp. 72–82

4 YU, Z.Z., PEYTON, A.J., BECK, M.S., and XU, L.A.: 'Electromagnetic tomography (EMT): A new process imaging system'. Proceedings of Sensor and applications VI, Manchester, UK, 12–15 Sept. 1993, (IOP Publishing), pp. 347–352

5 AL-ZEIBAK, S., and SAUNDERS, N.H.: 'Feasibility study of in vivo electromagnetic imaging', *Phys. Med. Biol.*, 1993, **38**, pp. 151–160

24

IEE Proc.-Sci. Meas. Technol., Vol. 145, No. 1, January 1998

6 HUANG, S.M., XIE, C.G., THORN, R., SNOWDEN, D., and BECK, M.S.: 'Design of sensor electronics for electrical capacitance tomography', *IEE Proc. G*, Feb. 1992, **139**, (1), pp. 83–88

7 XIE, C.G., HUANG, S.M., HOYLE, B.S., THORN, R., LENN, C., SNOWDEN, D., and BECK, M.S.: 'Electrical capacitance tomography for flow imaging, system model for development of image reconstruction algorithms and design of primary sensors', *IEE Proc. G*, Feb. 1992, **139**, (1), pp. 89–98

8 YU, Z.Z., PEYTON, A.J., BECK, M.S., CONWAY, W.F., and XU, L.A.: 'Imaging system based on electromagnetic tomography (EMT)', *Electron. Lett.*, 1 Apr. 1993, **29**, (7), pp. 625–626

9 PEYTON, A.J., YU, Z.Z., LYON, G.M., AL-ZEIBAK, S., XIONG, H.L., BORGES, A.R., SAUNDERS, N.H., and BECK, M.S.: 'An overview of electromagnetic inductance tomography, description of three different systems', *Meas. Sci. & Technol.*, 1996, **7**, pp. 216–271

10 WANG, M., DICKIN, F.J., and WILLIAMS, R.A.: 'Modelling and analysis of electrically conductive vessels and pipelines in electrical resistance process tomography', *IEE Proc. Sci. Meas. Technol.*, July 1995, **142**, (4), pp. 313–322

11 GISSER, D.G., ISAACSON, D., and NEWELL, J.C.: 'Current topics in impedance imaging', *Clin. Phys. Physiol. Meas.*, 1987, **Suppl. 8**, pp. A 39–46

12 YU, Z.Z.: 'Non-intrusive inductance based electromagnetic tomography (EMT) techniques for process imaging'. PhD thesis, UMIST, UK, 1994

13 PEYTON, A.J., YU, Z.Z., AL-ZEIBAK, S., SAUNDERS, N.H., and BORGES, A.R.: 'Electromagnetic imaging using mutual inductance tomography, potential for process applications', *Particles & Particle Syst. Character.*, 1995, **12**, pp. 68–74

14 REKTORYS, K.: 'Survey of applicable mathematics' (Iliffe Books, London, 1969)

IEE Proc.-Sci. Meas. Technol., Vol. 145, No. 1, January 1998

25